

Viscous Flow Simulation of Rotor Blades With Tip Slots in Hover

Ju Yeol You¹

Graduate Research Assistant

Oh Joon Kwon²

Professor

Yong Oun Han³

Professor

Department of Aerospace Engineering
Korea Advanced Institute of Science and Technology
Daejeon, KOREA

School of Mechanical Engineering
Yeungnam University
Gyongsan, KOREA

¹e-mail: aerodoctor@kaist.ac.kr ²e-mail: ojkwon@kaist.ac.kr

³e-mail: yohan@yu.ac.kr

Key words: Rotor blades, Slotted tip, Hover, Viscous flow simulation, Unstructured meshes

Abstract: The effect of tip slots on the tip vortex formation of a rotor blade in hover has been numerically investigated using unstructured meshes. The slots imbedded inside the blade surface were physically modelled and the flow through the slots was simulated as a part of the numerical solution. The mass flow rate through the slots was estimated at the slot exits, and the effect of slot position and the number of slots on the tip-vortex initial roll-up mechanism and the core structure was examined. The vorticity contours inside the tip-vortex core showed that the tip vortex generated from the slotted blade was more diffusive than that of the baseline rotor blade. It was found that for the slotted blade, the maximum vorticity level of the tip-vortex core was much lower than the baseline blade from the initial roll-up stage. It was also found that the tip-vortex core of the slotted blade was less well organized and was scattered more in an irregular pattern. As a result, the rate of vorticity diffusion of the slotted blade was much higher than the baseline blade. This effect was further magnified as the number of slots increased, and also as the Reynolds number and the blade tip Mach number increased. It was demonstrated that the tip slots can be used effectively to reduce the tip-vortex strength and to potentially alleviate the BVI noise of helicopter rotor blades.

INTRODUCTION

The tip vortex of three-dimensional wings induces strong downwash along the wing span and increases the aerodynamic drag by changing the effective angle-of-attack distribution. The flow field around helicopter rotors is much more complicated than that of fixed wings, since the tip vortex remains closely underneath the rotor disk and strongly affects the rotor blade performance. The interaction between the tip vortex and the rotor blades is referred as the blade-vortex interaction (BVI) [1, 2], which is the main source of the sudden change in the blade aerodynamic loading, the blade vibration, the aeroelastic instability, and the highly directional impulsive noise. Several research works have been previously conducted not only to understand the detailed mechanism of this complex phenomenon, but also to alleviate its adverse effect on the rotor aerodynamic performance.

Control of the tip vortex of rotor blades can be achieved by using either passive control devices or active control devices. Passive control devices utilize sub-wings, winglets, or spoilers to diffuse the tip vortex and to lower its strength [3, 4]. Active control devices adopt blowing or discrete tip jets, and directly control the flow by interrupting the cohesion of the tip vortex and reducing the swirl velocity [5, 6]. A numerical study has been conducted for the

comparison of the effects between passive and active control devices [7]. Even though both types of devices are effective in controlling the blade tip vortex, undesirable side effects, such as the loss in the aerodynamic performance and the additional structural penalties, also exist. Thus, a device which enables an effective control of the tip vortex without intolerable performance degradation is necessary for the design of future advanced helicopters.

Recently, experimental studies have been conducted for the investigation of the usefulness of tip slots as a mean of passive control device for alleviating the blade tip-vortex strength [8, 9]. In these studies, an array of slots were imbedded inside the blade surface at the blade tip region such that the flow is induced through the openings of the slots inserted at the blade leading edge and is ejected out from the tip vents at the side edge of the blade tip. The smoke visualization studies and the swirl velocity measurements inside the tip-vortex core showed that slotted tips rapidly diffuse the blade tip vortex, and as a result the vortex-induced unsteady airload and the BVI noise can be potentially alleviated, without a significant loss of the aerodynamic performance. However, the detailed physical mechanism of the flow through the slots and around the slotted tip has not been investigated.

A numerical study has been conducted for the investigation of the effect of tip blowing based on structured meshes [10]. In this study, two types of blowing, spanwise and streamwise, were adopted. The results showed that both blowing methods worked well, but the spanwise blowing was more effective. However, the blowing effect in this numerical study was modelled as a boundary condition imposed at the blade surface of the tip side edge, without considering the flow through the slots. A numerical study has also been conducted to study the effect of slots by physically simulating the flow through the slots [11]. The results showed that the flow from the slots has a significant effect on the formation of the blade tip vortex and the decay of the near-field tip-vortex strength. However, the calculations were limited to inviscid Euler flows, and thus the realistic viscous flow effect was not examined.

In the present study, the effect of slots on the blade tip-vortex formation has been numerically investigated by using a viscous flow solver on unstructured meshes. The slots imbedded inside the blade surface were realistically modelled by the computational mesh, and the flow through the slots was calculated as a part of the solution. Calculations were performed for both baseline and slotted blade configurations in hover [8], and the effects of the number of slots and the slot position on the tip-vortex initial formation and the core development were studied. Calculations were also performed for the investigation of the effects of the blade tip Mach number and the Reynolds number.

NUMERICAL METHOD

Discretization of Governing Equations

The equations governing three-dimensional, viscous, compressible flows are the Reynolds-averaged Navier-Stokes equations which express the conservation of mass, momentum, and energy for a Newtonian fluid in the absence of external forces. The equations can be recast on meshes moving through an inertial reference frame by using the absolute flow variables. The equations may be written in an integral form for a bounded domain V with a surface boundary ∂V :

$$\frac{\partial}{\partial t} \iiint_V Q dV + \iint_{\partial V} F(Q) \cdot \vec{n} dS = \iint_{\partial V} G(Q) \cdot \vec{n} dS + \iiint_V S(Q) dV \quad (1)$$

where $Q=[\rho, \rho u, \rho v, \rho w, e_0]$ is the vector of the conservative flow variables. These flow variables were normalized by the freestream density, the freestream speed of sound, and the blade chord length. The governing flow equations were discretized by using a cell-centered finite-volume method on unstructured meshes [12]. The inviscid flux, $F(Q)$, was computed using Roe's flux-difference scheme [13]. To achieve a second-order spatial accuracy, estimation of the state at each cell face was calculated by interpolating the solution using the Taylor series expansion in the neighborhood of each cell center [14]. The first derivatives of the viscous flux, $G(Q)$, were evaluated by using a linear reconstruction method [15]. The source term, $S(Q)$, was introduced to incorporate the blade rotation on the moving reference frame. The discretized linear system of equations was solved using an implicit point Gauss-Seidel iteration method.

The Spalart-Allmaras one-equation turbulence model [16] was adopted for the estimation of the turbulent eddy viscosity. In the present implementation, the turbulence model equation was solved separately from the mean flow equations by using the same time integration scheme, which resulted in a loosely coupled system.

The flow solver was parallelized by partitioning the computational domain into several subdomains using the MeTiS library. Communication of the data between the processors was achieved by using the MPI(Message Passing Interface) library. For the present cell-centered scheme, the data communication across the subdomain boundary was made for the flow variables at the nodes, at the face centers, and at the centroids of the adjacent cells.

Boundary Condition

In the present study, to relieve the stiffness of the solution related to the highly-stretched high aspect-ratio cells near the solid surface, a semi-empirical wall-function boundary condition was imposed on the surface of the blade.

At the far-field boundary, the pressure was fixed to the freestream value and the other flow variables were extrapolated from the interior. The value of the working variable for the Spalart-Allmaras turbulence equation was extrapolated from the interior for outflows and was specified to be a freestream value at the inflow boundary. The magnitude of freestream turbulence was set to 10 percents of the laminar viscosity.

BLADE MODELLING

The flow domain around the rotor blade was modelled by using unstructured meshes consisted of tetrahedral elements. The slotted blades were also modelled in a similar manner by additionally dividing the flow domain inside the slots with tetrahedral elements. The rotor blade configurations with and without the slots chosen in the present study were the same as those used in the experimental study [8]. The rotor was made of single untwisted rectangular blade with an NACA2415 airfoil section and an aspect ratio of nine. The blade root cut-out was 18 percents of the blade span. Each slot had geometry of a 90-degree-bent circular arc connecting the entrance at the blade leading edge and the exit at the tip side edge. The centers of the slot entrances were aligned along the blade leading edge at 17.8%, 33.4%, 49.0% and 64.6% chord lengths inboard from the blade tip. The exits of the slots at the blade tip side edge were also located at the same distances away from the blade leading edge, respectively,

and were aligned at 1.1% chord lengths above the chord line. Each slot had a circular section with a diameter of 6.7% chord lengths.

In Fig. 1, the surface triangulations on the baseline blade and the blade with four slots are presented. The mesh distribution around the slotted blade at the rotor disk plane is also shown in the figure. The computational meshes were composed of 3,027,094 tetrahedral cells and 518,642 nodes for the baseline rotor blade, and 3,558,103 tetrahedral cells and 611,463 nodes for the four-slot blade. The meshes for the blades with a different number of slots were also similar to those shown in the figure. To capture the initial roll-up and the formation of the tip vortex more accurately, dense cells were distributed near the blade tip region and along the tip vortex trajectory. The slot entrances along the blade leading edge, the exits at the blade tip side edge, and the circular arc passage of the slots inside the blade surface are visually confirmed in the figure.

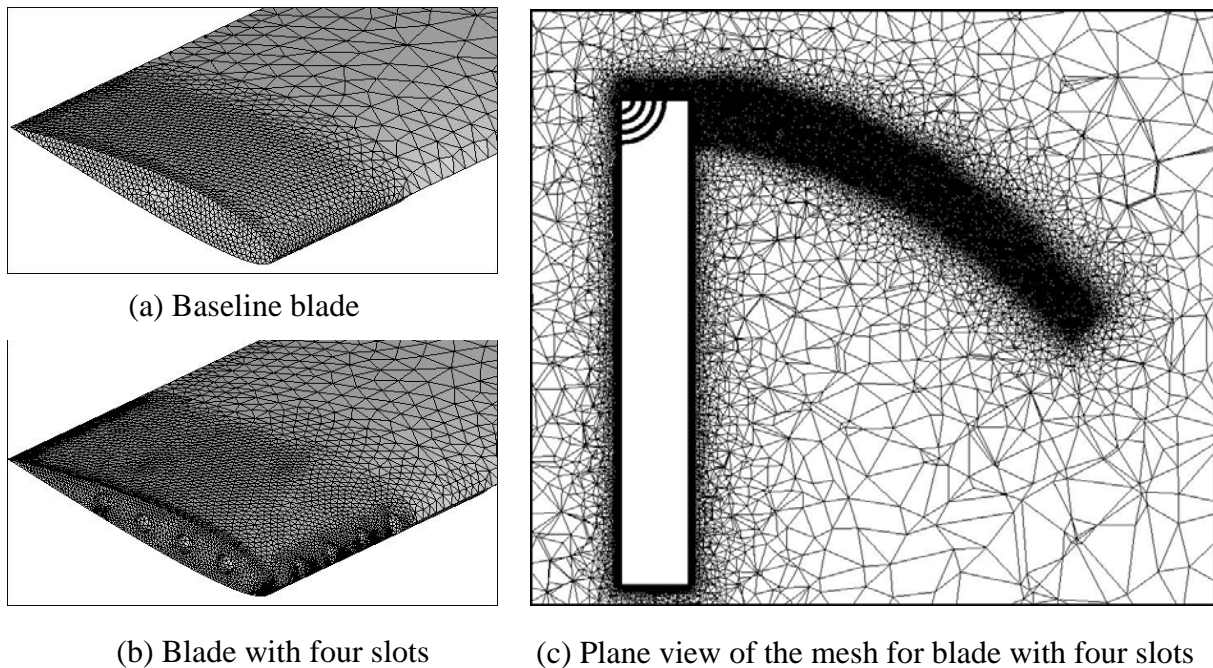


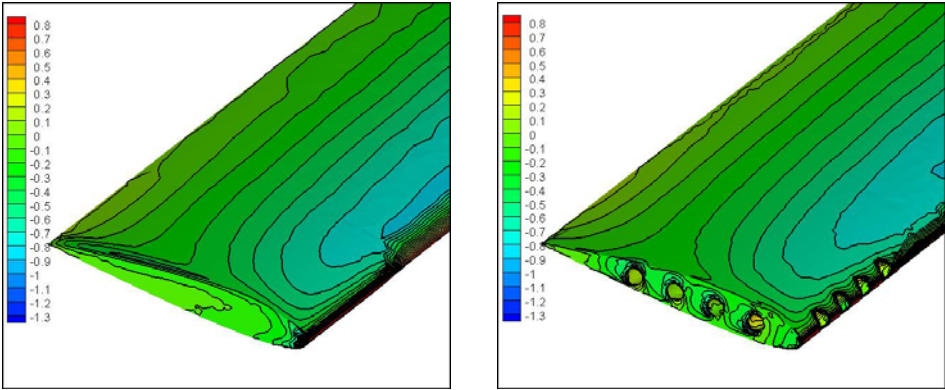
Fig. 1. Surface triangulation on baseline and slotted blade surfaces and field mesh.

RESULTS AND DISCUSSION

Effect of Number of Slots

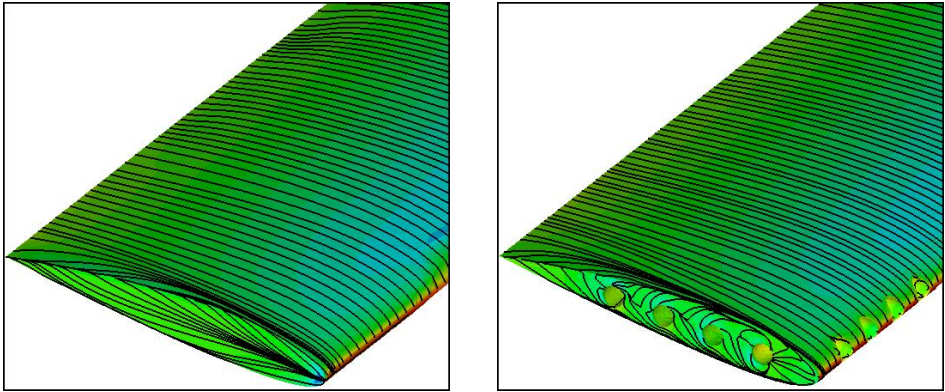
Initially, the baseline rotor blade without slots was calculated. Then, the blade with four slots was simulated. The rotor operating condition was chosen to be the same as the one adopted in the experimental study [8], which was at a blade tip Mach number of 0.26, a collective pitch angle of four degrees, and a Reynolds number of 2.72×10^5 . After the calculations converged, the predicted rotor thrust coefficient of the baseline blade was 0.00212, while that of the measurement was 0.002 [8]. The predicted thrust coefficient of the rotor blade with four slots was 0.00204, approximately three percent less than that of the baseline rotor blade. The predicted torque coefficient of the baseline blade was 0.000272, and that of the four-slot blade was 0.000249 which was approximately eight percents less than the baseline blade.

The pressure coefficient contours on the surface of the baseline and slotted rotor blades are compared in Fig. 2. It shows that the overall pressure distributions were similar to each other, except where the slot entrances and exits were located. Because of the pressure difference between the slot entrance at the blade leading edge and the slot exit at the tip, flow was induced into the slot entrance and ejected from the exit without any active energy supply mechanism.



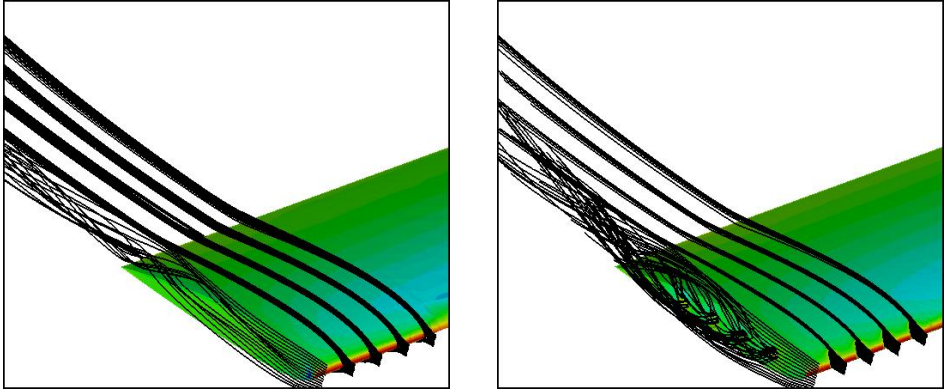
(a) Baseline blade (b) Blade with four slots

Fig. 2. Comparison of surface pressure contours between baseline and slotted blades.



(a) Baseline blade (b) Blade with four slots

Fig. 3. Comparison of surface streamline traces between baseline and slotted blades.



(a) Baseline blade (b) Blade with four slots

Fig. 4. Comparison of streamline traces around the blade tip region between baseline and slotted blades.

In Fig. 3, the streamline traces on the blade surface are compared between the baseline blade and the slotted blade. It shows that blowing of flow from the slot exits created a rather complicated flow pattern at the blade tip, demonstrating that the tip vortex formation was less well organized than that of the baseline blade. This tendency was also well demonstrated in Fig. 4 which represents the comparison of the field streamline traces between the baseline blade and the slotted blade.

To examine the effect of the number of slots, the blades with different number of slots were calculated. For the blades with single slot, each slot of the four-slot blade was individually considered. In the case of the blade with two slots, the second and third slots of the four-slot blade were examined. Also, for the simulation of the blade with three slots, the three slots except the first one were implemented on the blade. The results are presented as the mass flow rate out from the slot exit in Table 1. The mass flow rate was normalized by the freestream density, the square of the chord length, and the freestream speed of sound. It shows that for the blades with single slot, the largest mass flow rate was observed from the slot located closest to the leading edge. This is because the pressure difference between the slot entrance and the exit was the largest at outboard because of the high stagnation pressure at the leading edge. In the case of multiple slots, the mass flow out from the second slot was always the largest. This is presumably due to the fact that the flow ejected from the first slot behaved as a blockage to the main stream, and thus a low pressure region was formed at the downstream where the other slot exits were located. As a consequence, the pressure difference between the slot entrance and the exit increased at the subsequent slots, inducing higher mass flow rate. In overall, the total mass flow rate from the slots increased as the number of slots increased. From the mass-flow-rate observation, it was expected that different combination of slots in number and position may be used to adjust the total mass flow rate and subsequently to control the tip vortex behaviour.

Blade type	Mass flow rate ($\times 10^{-3}$)			
	Slot 1	Slot 2	Slot 3	Slot 4
1 st slot only	0.4112	-	-	-
2 nd slot only	-	0.3702	-	-
3 rd slot only	-	-	0.3628	-
4 th slot only	-	-	-	0.3401
Two slots	-	0.3498	0.5620	-
Three slots	-	0.3389	0.5415	0.4707
Four slots	0.4921	0.5453	0.4698	0.4053

Table 1. Comparison of mass flow rate through slots.

In Fig. 5, vorticity contours at the sectional plane across the tip-vortex core are compared between the baseline blade and the slotted blade at several near-field wake ages. It shows that the flow ejected from the slot exits had an effect of enlarging the tip-vortex core size and making the core less well organized than that of the baseline blade. This behaviour became more evident as the number of slots increased. As the tip vortex migrated downstream away

from the blade, the vorticity of the tip-vortex core of the slotted blades was quickly diffused and the maximum vorticity level became much less than that of the baseline blade. This tendency was further magnified as the number of slots increased, demonstrating higher effectiveness in controlling the tip vortex. In Table 2, the maximum vorticity level inside the tip-vortex core is compared between the baseline blade and the blade with four slots. It shows that in the case of the slotted blade, the maximum vorticity level of the tip vortex was significantly lower than that of the baseline blade. Also, the vorticity level of the slotted blade was diffused in a much higher rate than the baseline blade.

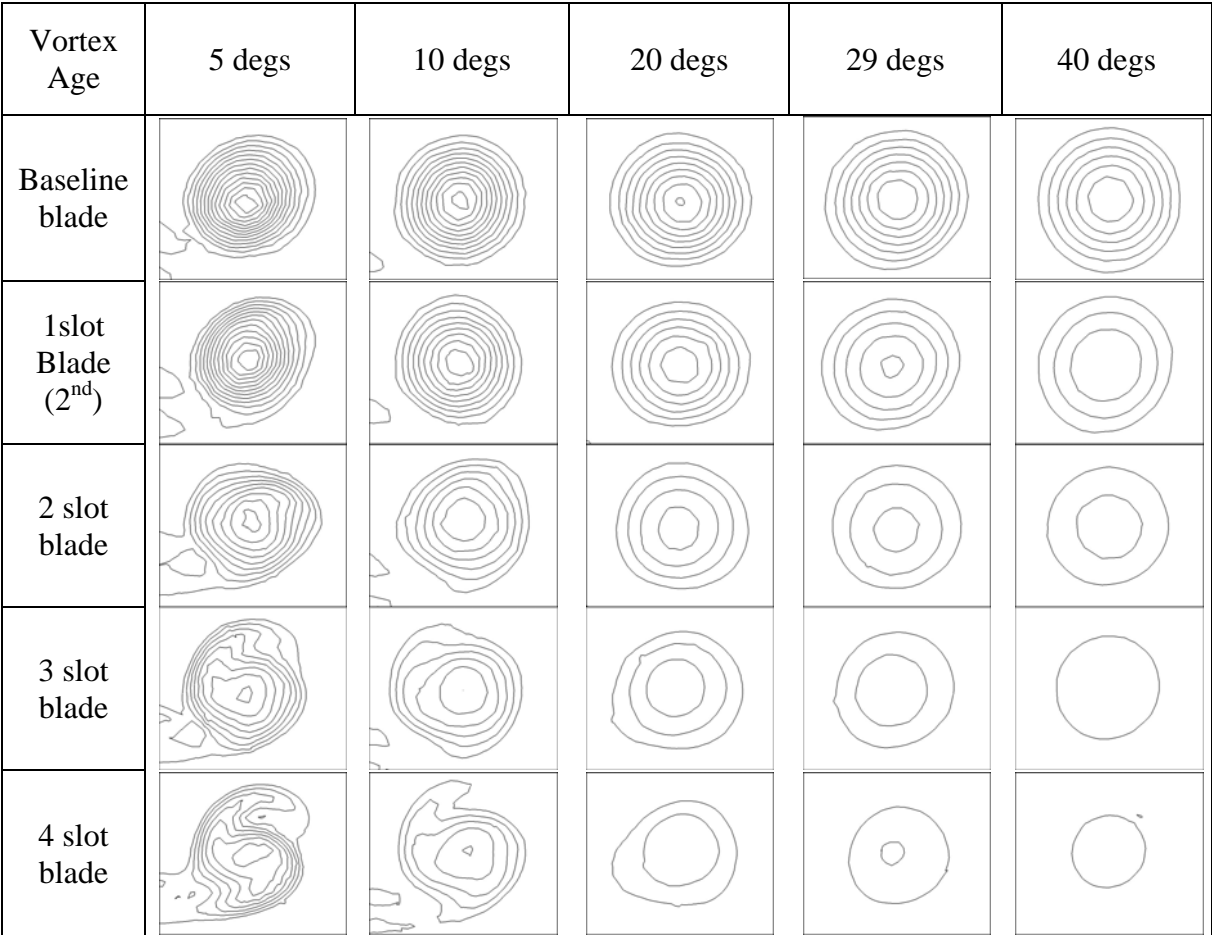


Fig. 5. Comparison of vorticity contours inside the near-field tip-vortex core.

Vortex Age	5 degs	10 degs	20 degs	29 degs	40 degs
Baseline blade	1.9786	1.6767	1.3730	1.1940	1.0696
4 slot blade	1.1513	0.8428	0.5600	0.4411	0.3504

Table 2. Normalized maximum vorticity level inside the tip vortex core.

In Fig. 6, the swirl velocity distributions inside the tip-vortex core are compared between the present calculation and the experiment [8] at the wake age of 29 degrees. It shows that the predicted results are in reasonable agreement with the measurement for both the peak value

and the overall distribution. The predicted peak values were slightly higher than the measurement for both the baseline and four-slot blades. Also, the predicted core sizes of both blade cases were slightly larger than the measurement. The results show that the effect of slots was mostly on enlarging the core size and reducing the peak value, while the overall swirl velocity distribution outside the vortex core remained mostly unchanged.

In Fig. 7, the detailed flow behaviour inside the slots was examined by the surface streamline traces along the slot wall. It shows that the flow separated from the sharp edge of the slot entrance. This separated flow quickly re-attached at the downstream, and then relatively smooth flow was observed throughout the rest of the slot channel. The flow showed a helical motion rotating counter-clockwise as it travelled downstream toward the slot exit. The rotational direction of the slot flow was opposite to that of the tip vortex. Thus, when the flow out from the slots was added into the tip vortex, multiple cores of locally counter-rotating flows were obtained inside the tip vortex. This phenomenon physically explains the formation of the expanded vortex core structure observed for the slotted blade in Fig. 5 and also the vorticity behaviour discussed earlier for the results in Table 2.

Effect of Reynolds Number and Tip Mach Number

The results presented in the previous section were calculated for a relatively low tip Mach number of 0.26 and a low Reynolds number of 2.72×10^5 to match the flight condition to that of the experiment [8]. However, it is obvious that practical helicopter rotors operate at higher blade tip Mach numbers and Reynolds numbers. To examine the effect of the tip slots at more realistic operating conditions, calculations were performed by increasing the blade tip Mach number and the Reynolds number to 0.877 and 3.93×10^6 , respectively. This is the same operating condition adopted in the experiments for a hovering rotor by Caradonna and Tung [17]. At first, the effect of Reynolds number was tested by increasing the value to 3.93×10^6 , while the blade tip Mach number was fixed to the previous subsonic Mach number of 0.26.

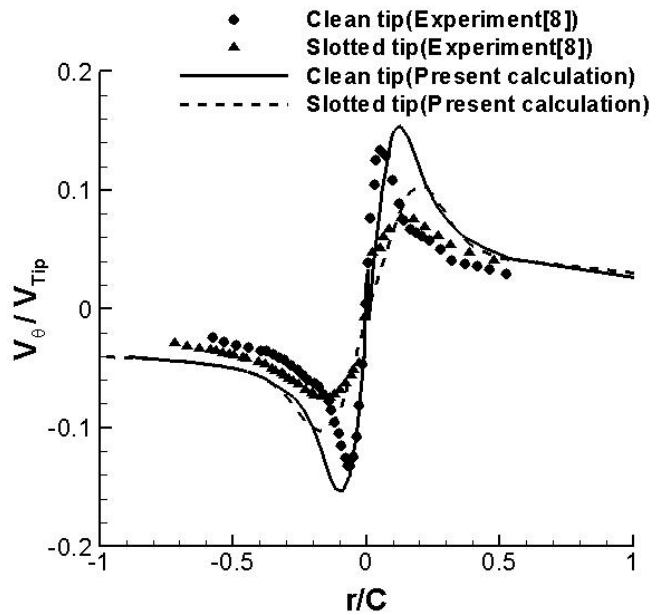


Fig. 6. Comparison of normalized swirl velocity inside the tip-vortex core at 29 degree wake age.

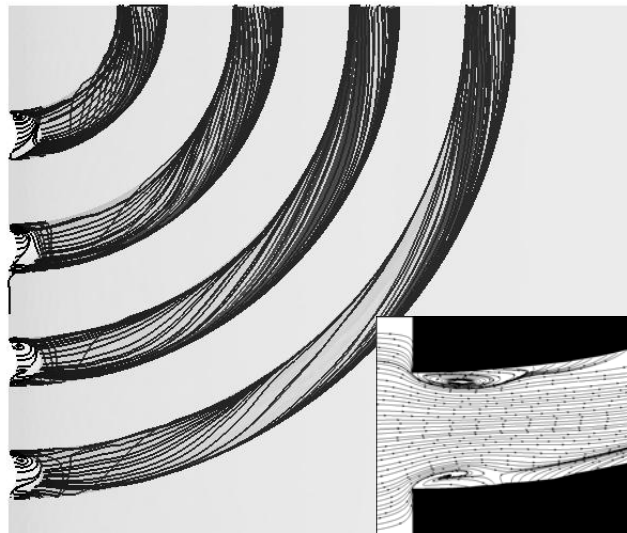
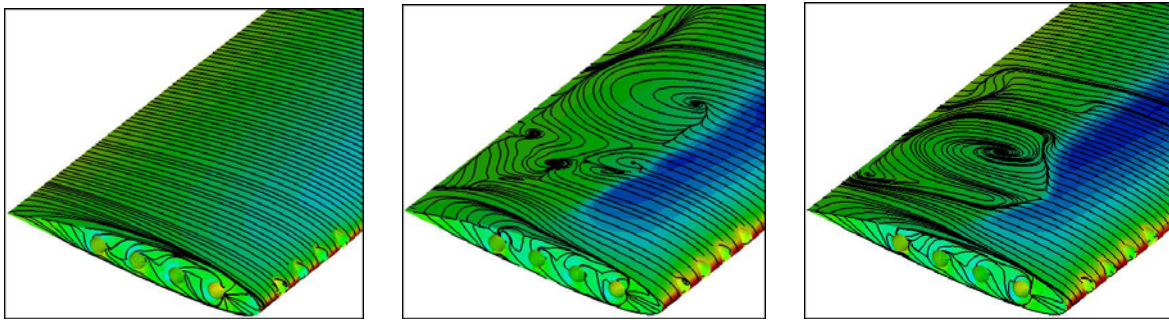


Fig. 7. Surface streamline traces inside the slots and a magnified view of field streamlines at the slot entrance.

Next, the blade tip Mach number was increased to 0.877, while the Reynolds number was fixed as it was at 2.72×10^5 . Then, the blade tip Mach number and the Reynolds number were simultaneously increased to 0.877 and 3.93×10^6 , respectively. All three calculations were performed for the blade with four slots.

In Fig. 8, the surface streamline traces are presented for all three cases. It shows that increasing the Reynolds number at the fixed subsonic tip Mach number did not affect the flow significantly, and the flow remained attached on the blade surface, similar to that of the lower Reynolds number case presented in Fig. 3. When the blade tip Mach number was increased to the transonic speed, a strong shock wave appeared on the upper surface of the blade, and shock-induced local flow separation was observed for both transonic tip Mach number cases. Because of the increased tip speed, the leading-edge stagnation pressure increased higher than that of the subsonic case, and thus it was expected that more mass of flow was induced into the slots. As a result, at this transonic tip speed, the tip-vortex core size of the slotted blade was further enlarged. The effect is shown on the streamline traces at the tip region near the trailing edge.



(a) $M_{tip}=0.26$, $Re=3.93 \times 10^6$ (b) $M_{tip}=0.877$, $Re=2.72 \times 10^5$ (c) $M_{tip}=0.877$, $Re=3.93 \times 10^6$

Fig. 8. Effect of Reynolds number and tip Mach number on surface streamline traces and pressure contours.

In Table 3, the normalized mass flow rates through the slots are presented for the three rotor operating conditions. Compared to the results for the four-slot blade in Table 1, the mass flow rate slightly increased when the Reynolds number increased. However, when the tip Mach number increased from subsonic to transonic, a significant increment of the mass flow rate was obtained, showing that the effect of slots became more evident as the blade tip Mach number increased.

Flow cases	Mass flow rate ($\times 10^{-3}$)			
	Slot 1	Slot 2	Slot 3	Slot 4
$M_{tip}=0.26$ $Re = 3.93 \times 10^6$	0.4744	0.5999	0.5393	0.4859
$M_{tip} = 0.877$ $Re = 2.72 \times 10^5$	1.9757	2.0073	1.8869	1.7444
$M_{tip} = 0.877$ $Re = 3.93 \times 10^6$	2.0596	2.1455	2.0624	1.9394

Table 3. Effect of Reynolds number and tip Mach number on mass flow rate through slots.

In Fig. 9, vorticity contours at the sectional plane across the tip-vortex core are presented for the three rotor operating conditions. Compared to the results of the subsonic tip Mach number and the low Reynolds number in Fig. 5, it was observed that the effect of slots became more significant when the tip Mach number increased from subsonic to transonic. The tip-vortex core exhibited higher vorticity level and showed a structure less well organized and widely spread, not only at the initial formation stage but even at further downstream. The effect of increasing the Reynolds number was relatively not as significant, compared to that of compressibility. In Table 4, the maximum vorticity level inside the tip-vortex core is presented for the three rotor operating conditions. The results again demonstrated the effect of increasing the Reynolds number and the tip Mach number for the slotted blade. It was also observed that the decay rate of vorticity in terms of the wake age was more severe as the tip Mach number increased.

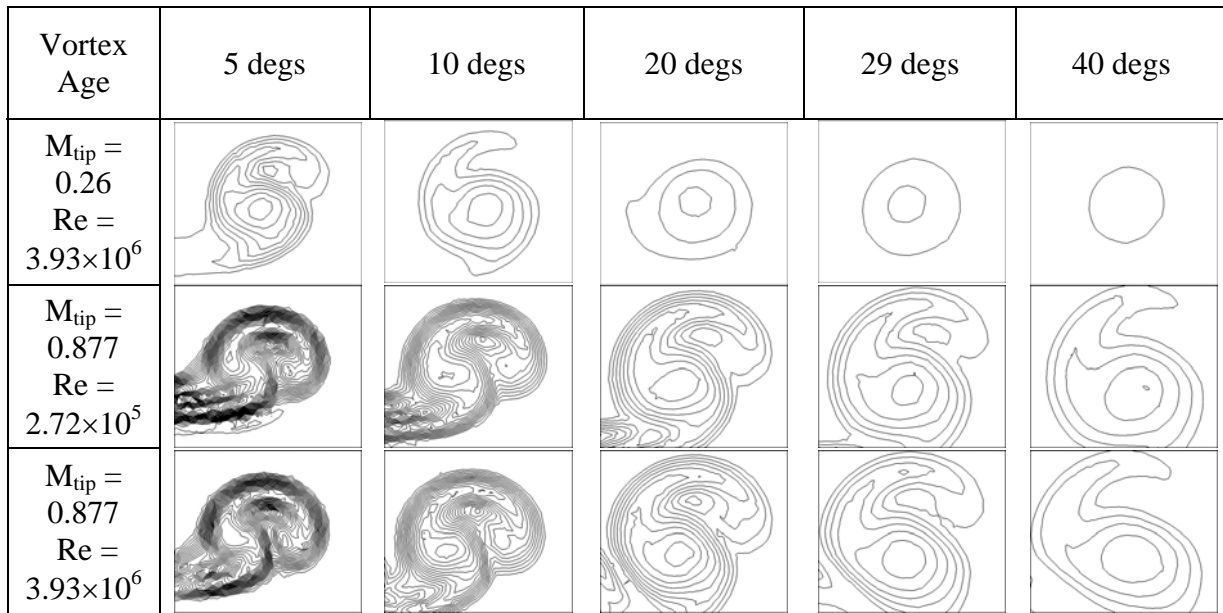


Fig. 9. Effect of Reynolds number and tip Mach number on vorticity contours inside the near-field tip-vortex core.

Vortex Age	5 degs	10 degs	20 degs	29 degs	40 degs
$M_{tip}=0.26$ $Re = 3.93 \times 10^6$	1.2950	0.9261	0.5906	0.4582	0.3613
$M_{tip} = 0.877$ $Re = 2.72 \times 10^5$	3.4775	2.1801	1.3220	1.0040	0.8689
$M_{tip} = 0.877$ $Re = 3.93 \times 10^6$	3.6130	2.3310	1.4071	1.0632	0.8014

Table 4. Effect of Reynolds number and tip Mach number on normalized maximum vorticity level inside the tip-vortex core.

In Fig. 10, the normalized swirl velocity distributions inside the tip-vortex core are compared at the wake age of 29 degrees for the three rotor operating conditions. It shows that when the Reynolds number increased from 2.72×10^5 to 3.93×10^6 , the swirl velocity distribution did not

change much. However, when the tip Mach number increased from 0.26 to 0.877, a significant increment of the peak values was observed. Also, at the transonic tip Mach number, the tip-vortex core exhibited multiple peaks at the inboard section, representing that the core was not tightly organized as it was also observed on the vorticity contours in Fig. 9. This demonstrated that the effect of slots on the tip vortex remained for a significantly longer period of time at high tip Mach numbers.

In Fig. 11, the local Mach number contours are presented inside the slots and around the blade tip region at the blade tip Mach number of 0.877 and the Reynolds number of 3.93×10^6 . It shows that the flow slightly accelerated as it travelled through the slot channel and reached a near-sonic speed at the slot exit region. This high-speed flow was more evident for the slots located closer to the blade leading edge. However, formation of shock waves inside the slot channels was not observed, at least for the blade tip Mach number tested in the present study.

CONCLUDING REMARKS

In the present study, the effect of slots on the tip-vortex formation of a rotor blade in hover has been numerically investigated on unstructured meshes. The mass flow rates through the slots were evaluated at the exit of the slots, and the effect of slot position and the number of slots on the tip-vortex initial roll-up mechanism as well as the core structure was studied. The streamline traces and the vorticity contours showed that the tip vortex of slotted blades was less well organized and diffused faster than the baseline blade because of the mass injected from the slots. For the slotted blades, the maximum vorticity level of the tip-vortex core was initially lower than that of the baseline blade, and also the level was reduced at a much higher rate compared to the baseline blade. This tendency was further magnified as the number of slots increased. The effect of slots became more evident as the blade tip Mach number and the Reynolds number increased. It was found that the tip vortex and its vorticity strength may be controlled by adjusting the number of slots and possibly their positions, without a significant loss of the rotor aerodynamic performance, for the potential alleviation of BVI noise.

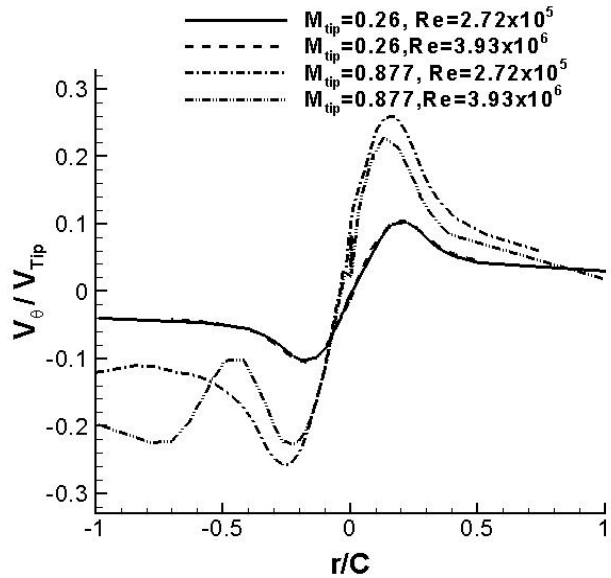


Fig. 10. Effect of Reynolds number and tip Mach number on normalized swirl velocity distribution inside the tip-vortex core at 29 degree wake age.

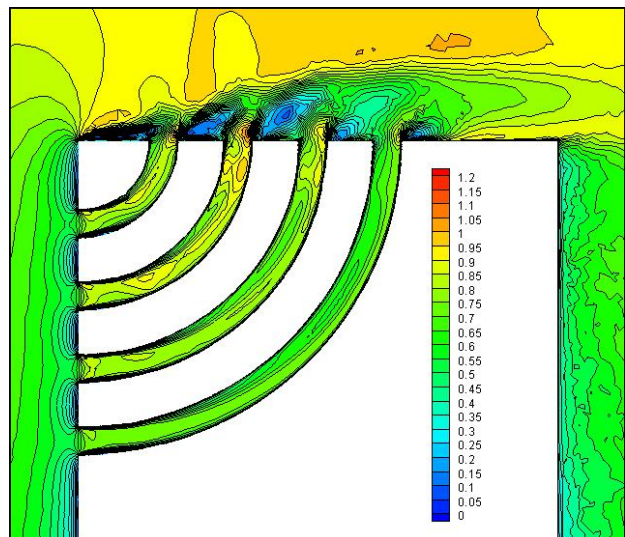


Fig. 11. Mach number contours inside the slots and around the blade tip region at $M_{tip}=0.877$ and $Re=3.93 \times 10^6$.

ACKNOWLEDGMENTS

This study has been supported by the KARI under KHP Dual-Use Component Development Program funded by the MOCIE.

REFERENCES

- [1] Leishman, J., and Bagai, A., "Challenges in Understanding the Vortex Dynamics of Helicopter Rotor Wakes," *AIAA Journal*, Vol. 36, No. 7, 1998, pp. 1130-1140.
- [2] Leishman, J. G., *Principles of Helicopter Aerodynamics*, Cambridge University Press, New York, 2006.
- [3] Tangler, J. L., "Experimental Investigation of the Sub-wing Tip and its Vortex Structure," NASA CR-3058, 1978.
- [4] Smith, D. E., and Sigl, D., "Helicopter Rotor Tip Shapes for Reduced Blade Vortex Interaction," AIAA Paper 95-0192, 1995.
- [5] Gowanlock, D. K., and Matthewson, C. S., "Control of Rotor Tip Vortices," AIAA Paper 99-0012, 1999.
- [6] Sarpkaya, T., "Vortex Breakdown & Turbulence," AIAA Paper 95-0433, 1995.
- [7] Liu, Q., Russel, J. W., Sankar, L. N., and Hassan, A. A., "A Study of Rotor Tip Vortex Structure Alteration Techniques," *Journal of Aircraft*, Vol. 38, No.3, May 2001, pp. 473-477.
- [8] Han, Y. O., and Leishman, J. G., "Investigation of Helicopter Rotor-Blade-Tip-Vortex Alleviation Using a Slotted Tip," *AIAA Journal*, Vol. 42, No. 3, March 2004, pp. 524-535.
- [9] Han, Y. O., and Leishman, J. G., "Hovering Performance of a Rotor with Slotted Blade Tips," American Helicopter Society 60th Annual Forum Proceedings, Baltimore, MD, June 7-11, 2004.
- [10] Duraisamy, K. and Baeder, J. D., "Control of Helicopter Rotor Tip Vortex Structure Using Blowing Devices," American Helicopter Society 60th Annual Forum Proceedings, Baltimore, MD, June 7-11, 2004.
- [11] Park, Y. J., Kwon, O. J., and Han, Y. O., "Numerical Investigation of the Effect of Slots on Rotor Blade Tip Vortex Formation," Proceedings of the 2nd International Basic Research Conference on Rotorcraft Technology, Nanjing, China, Nov. 7-9, 2005, pp. 135-143.
- [12] Kang, H. J., and Kwon, O. J., "Unstructured Mesh Navier-Stokes Calculations of the Flow Field of a Helicopter Rotor in Hover," *Journal of the American Helicopter Society*, Vol. 47, No. 2, April 2002, pp. 90-99.
- [13] Roe, P. L., "Approximate Riemann Solvers, Parameter Vectors and Difference," *Journal of Computational Physics*, Vol. 43, 1981, pp. 357-372.
- [14] Frink, N. T., "Upwind Scheme for Solving the Euler Equations on Unstructured Tetrahedral Meshes," *AIAA Journal*, Vol. 30, No. 1, 1992, pp. 70-77.
- [15] Mitchell, C. R., "Improved Reconstruction Schemes for the Navier-Stokes Equations on Unstructured Meshes," AIAA Paper 94-0642, 1994.
- [16] Spalart, P. R., and Allmaras, S. R., "A One-Equation Turbulence Model for Aerodynamics Flows," AIAA Paper 92-0439, 1992.
- [17] Caradonna, F. X., and Tung, C., "Experimental and Analytical Studies of a Model Helicopter Rotor in Hover," NASA TM81232, 1981.